Appl. Phys. B 87, 671–675 (2007)
DOI: 10.1007/s00340-007-2636-4

Applied Physics B
Lasers and Optics

C. SCURTESCU[1]
Z.Y. ZHANG[1]
J. ALCOCK[2]
R. FEDOSEJEVS[1]
M. BLUMIN[3]
I. SAVELIEV[3]
S. YANG[3]
H. RUDA[3]
Y.Y. TSUI[1,✉]

Quantum dot saturable absorber for passive mode locking of Nd:YVO_4 lasers at 1064 nm

[1] Department of Electrical and Computer Engineering, 2nd Floor, ECERF, University of Alberta, Edmonton, Alberta, Canada, T6G 2V4
[2] Institute for Microstructural Sciences, National Research Council of Canada, 1200 Montreal Road, Ottawa, Ontario, Canada, K1A 0R6
[3] Centre for Advanced Nanotechnology, University of Toronto, Haultain Bldg., 170 College Street, Toronto, Ontario, Canada, M5S 3E4

Received: 24 October 2006/Revised version: 26 February 2007
Published online: 9 May 2007 •

ABSTRACT An InAs/GaAs quantum dot saturable absorber mirror was used to mode lock a Nd:YVO_4 solid-state laser at the operation wavelength of 1064.6 nm. Multi-watt average power was obtained during stable cw mode locking with pulses as short as 24 ps, and with a repetition rate of 65 MHz.

PACS 45.55.-f; 78.67.Hc; 42.60.Fc

1 Introduction

The progress of the molecular beam epitaxy (MBE) and metal organic chemical vapor deposition (MOCVD) techniques has allowed the fabrication of good-quality self-organized quantum dot materials, and opened a new research direction on fundamental studies and potential device applications. In both fabrication techniques the dot size distribution is typically larger than 10%, which often limits the use of these quantum dot materials in cw lasers. On the other hand, QD-based devices with applications in the generation of ultra-short laser pulses take advantage of the broad gain/absorption spectrum of the quantum dot material, which is associated with the unavoidable dot size distribution. One such application is that of a fast saturable absorber for passive mode locking of a solid-state laser.

In addition to QD materials, quantum well (QW) materials can also be used as saturable absorbers. However, when a QW structure is used as a saturable absorber material [1, 2], it is necessary to grow it at lower temperature or perform post-growth ion implantation in order to obtain a fast absorber recovery time. These in turn not only shortens the absorption recovery time (which is advantageous for mode-locked operation), but also increases the nonsaturable losses (which is not desired). The use of ion implantation as an additional fabrication step will unavoidably introduce one more process step, and thus may reduce the overall device yield. This is disadvantageous for any potential commercial device. On the other hand, QD materials are expected to have ultra-fast dynamic response naturally without any additional constraints on fabrication [3].

✉ Fax: (780) 4921811, E-mail: tsui@ece.ualberta.ca

Recent development of quantum dot saturable absorber mirrors (QD-SAMs) [4–8] shows the significant potential of these structures for ultra-short laser pulse generation through passive mode locking. The QD-SAM is composed from a QD-based absorption section grown monolithically on top of a distributed Bragg reflector (DBR) and is used as an end mirror of a laser cavity for passive mode locking. The laser light enters into the QD-SAM, is selectively absorbed by the QD absorption section, and then reaches the DBR and is reflected back in the laser cavity passing again through the absorption section. The operation bandwidth of a saturable absorber mirror (SAM) is defined by the spectrum of the absorption material, by the high-reflectivity plateau of the distributed Bragg reflector, and by the Fabry–Pérot cavity formed between the Bragg reflector and the exit surface of the device. Due to the intensity-dependent saturation of absorption, the QD-based absorber will preferentially transmit high-intensity pulses in the laser cavity. Thus, it causes the laser to operate in a mode-locked fashion. In(Ga)As/GaAs QDs have already been used as a saturable absorber medium in QD-SAMs, and a few laser gain materials have been mode locked in the wavelength range 1.03–1.34 μm [4–8]. Moreover, the potential of using QD-based saturable absorbers in the communication window of 1.55 μm has been proposed [9]. As the substrate used is GaAs, these absorbers also benefit from the large index contrast of lattice-matched Al(Ga)As/GaAs DBRs. This DBR material system gives a broad high-reflectivity plateau with a reduced number of layers.

No experiments on mode locking a Nd:YVO_4 laser at $\lambda = 1064$ nm by using self-assembled QD saturable absorbers have been reported to date. Previous work on mode locking of a Nd:YVO_4 laser using QD saturable absorbers was done at $\lambda = 1342$ nm, using a 0.3% Nd doped crystal, and a 26-ps pulse width was obtained [6].

In the present paper we report the study of an InAs/GaAs QD saturable absorber to mode lock a Nd:YVO_4 laser at 1064.6 nm.

2 QD-SAM design and fabrication

The QD-SAM device presented here was monolithically grown on an n^+ (100)GaAs substrate by molecular beam epitaxy using a SemiTEq ATC-EP3 MBE system. The device has two main components, a QD-based saturable ab-

sorber and a DBR structure on which the saturable absorber is grown. A schematic diagram of the QD-SAM design is shown in Fig. 1. The fabrication process started with the growth of a 300-nm-thick GaAs buffer layer at 600 °C in order to improve the substrate planarity and reduce its surface defect density. Then, a sequence of 25 pairs of $\lambda/4$ AlAs/GaAs (90.6 nm/76.5 nm) layers was deposited at 580 °C to form a distributed Bragg reflector centered on $\lambda = 1064$ nm. To get high DBR reflectivity, it is necessary to obtain sharp interfaces between the layers. This can be achieved by allowing time for the added atoms to migrate on the crystal surface before the next layer of different material is deposited, but not too long to combine with the residual oxygen from the chamber. For this reason we have used a 60 s growth interruption after each GaAs layer and 40 s after each AlAs layer growth. Because the AlAs and GaAs materials are lattice matched, it has allowed the deposition of dislocation-free layers and prepared the surface for the growth of the self-assembled quantum dots.

Following the growth of the DBR, three groups of three layers of self-assembled InAs/GaAs QDs were grown. A thickness of 1.9 monolayers (ML) of InAs at 0.04 ML/s growth rate was used to form each of the nine InAs QD layers. A 20-nm GaAs layer separated the InAs QD layers within each group of QDs, and a 112-nm GaAs layer separated the individual groups. Finally, the structure was covered with a 132-nm GaAs layer. The As pressure during growth was 2.4×10^{-6} Pa, sufficient to ensure an As-stabilized surface, but low enough to allow good indium atom surface mobility before bonding with the As atoms. Similar As pressures have been reported in [10] to give high-quality self-assembled InAs/GaAs QDs. For QD materials deposited using similar parameters, the QDs are pyramidal in shape with a base of 15–20 nm and a height of 1.5–3 nm [11, 12].

Generally, in MBE growth, the parameters are designed for the center of the substrate, which is then continually rotated during growth in order to produce a good uniformity of the structure across the entire surface. Therefore, the amounts and ratios of different materials deposited on various positions of the substrate, from the differently located MBE effusion cells, will be similar. In the case when the substrate is not rotated during the growth process, the different material layers will have different thicknesses and ratios across the wafer. For the case of the QD-SAM this translates into a variation in the reflectivity spectrum of the DBR and a variation in the QD size (which determines the QD photoluminescence/absorption spectra) across the wafer. For the design presented here we used no substrate rotation.

3 QD-SAM characterization

The low-intensity reflectivity spectrum of the QD-SAM device has been measured at different points on the wafer. Due to the fact that no rotation was used during the growth, various reflectivity spectra have been obtained across the wafer [9]. The reflectivity measurements were performed at room temperature by using a Perkin-Elmer Lambda 900 UV/Vis/NIR dual-beam spectrometer, with the beam incidence angle on the sample of $\sim 10°$. The reflectivity calibration was realized with a commercial Au mirror where the reflectivity of the Au mirror was taken as 98% at these wavelengths [13]. From these, we have identified the area presented in Fig. 2 where the DBR high-reflectivity plateau shows a dip at $\lambda = 1061$ nm wavelength in the vicinity of the peak emission ($\lambda = 1064$ nm) of the Nd:YVO_4 laser that was used in the present experiment. In the reflectivity spectrum shown in Fig. 2 it can be observed that there is a 27% spectral dip in the reflectivity at $\lambda = 1061$ nm in the DBR high-reflectivity plateau. This dip is associated with absorption from the QDs together with the resonant Fabry–Pérot cavity of the absorber mirror and outer GaAs surface. The measurements show that the DBR high-reflectivity spectrum is > 70 nm wide.

The room-temperature photoluminescence (PL) emission from a QD test sample has been measured. The room-temperature QD PL was measured by using a 20-mW cw diode laser excitation source at 790.5 nm focused onto a circular spot of 260 μm FWHM on the sample. The spectral emission from the QDs was recorded using an Acton Research Corporation 500 spectrometer equipped with an NIR opti-

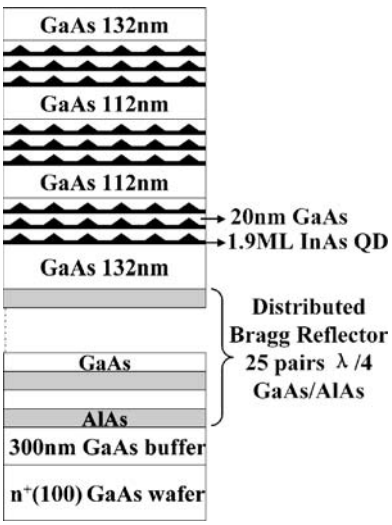

FIGURE 1 Schematic diagram of the QD-SAM

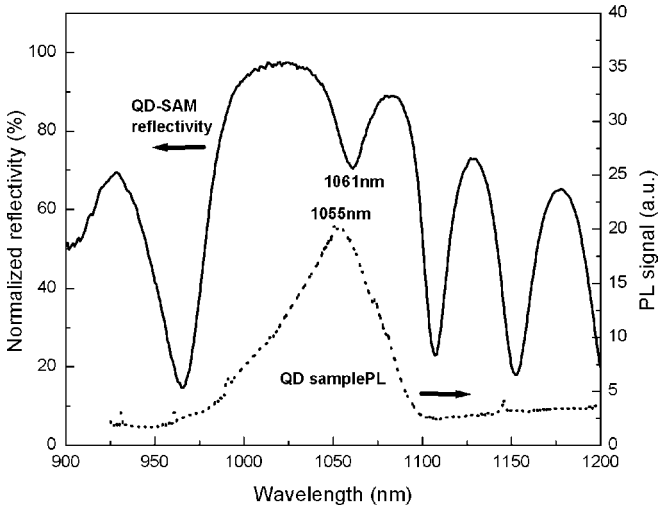

FIGURE 2 Low-intensity reflectivity spectrum of the QD-SAM and the room-temperature photoluminescence spectra of a QD test sample

cal multi-channel analyzer detector (InGaAs/InP 256-pixel CCD, model 1452NIR, Princeton).

Figure 2 shows the PL measurements from a QD test sample. The test sample contains 21 QD layers grown in similar conditions as the QDs from the QD-SAM device, and the PL measurements were performed in a similar area on the substrate with regard to the In source location. Interestingly, we have detected PL signals from both the QD structures and the GaAs substrate. In Fig. 2, the emission with the peak in the vicinity of 1055 nm and width of 60 nm FWHM corresponds to the QD photoluminescence, and the long wavelength range emission tail originates from the GaAs substrate luminescence due to the 790.5-nm pump laser. We have measured similar emission in the long-wavelength range on bare GaAs samples. It can be observed that the maximum in the PL spectrum is correlated with the dip in the reflectivity spectrum.

4 Nd:YVO_4 laser system

To investigate the QD-SAM device for passive mode locking we have implemented the laser setup shown in Fig. 3. The laser gain material consists of a Nd:YVO_4 slab with 1% Nd doping, which is optically side pumped by a laser diode array at $\lambda = 808$ nm. The pump optical power is variable up to a maximum measured value of 44.5 W. The pump beam was focused on the laser crystal by using the cylindrical lens L3 with $f = 12.7$ mm. The crystal side facing the pump was antireflection (AR) coated for $\lambda = 808$ nm. The Nd:YVO_4 crystal has a trapezoidal shape in the plane of the figure, with the largest side facing away from the pump laser diode array and with the end faces cut at 5° relative to normal. The exit and entrance faces of the laser crystal were AR coated for $\lambda = 1064$ nm for an angle of incidence of 0–20°. The entire assembly, pump-diode bar plus laser crystal, was kept at a constant temperature of 14.5 °C by the use of a water-cooling system, in order to control the pump wavelength and allow stable operation.

Two cylindrical lenses L1 and L2 (both with $f = 5$ cm) were used to confine the lasing mode to a narrow stripe within the slab (the cylindrical axes are in the plane of the figure). This geometry uses the total internal reflection on the pumped face of the slab in order to obtain a high degree of overlap between the lasing mode and absorbed pump radiation. The angle of incidence of the laser mode on the pumped face of the Nd:YVO_4 slab was approximately 5°. The Nd:YVO_4 crystal has an optimum absorption coefficient at ~ 808 nm, which is the wavelength of the pump diode array that we used. This configuration is known as a grazing incidence slab laser (GISL) [14–16], and has the advantages in achieving a high conversion efficiency of the pump power into lasing power, and high average output power.

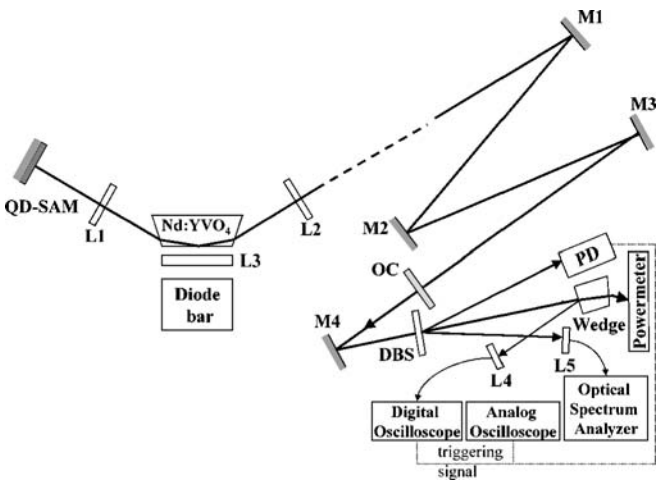

FIGURE 3 Schematic diagram of the mode-locked laser setup (L1–L5: lenses, M1–M4: dielectric mirrors; PD: photodiode; DBS: diffractive beam splitter; OC: output coupler)

The high-reflectivity laser end mirror was initially a broadband dielectric mirror that was later replaced with our QD-SAM for pulsed operation tests. The position of the end mirror could be adjusted in all three directions over a range of 2 cm for fine tuning during lasing operation. The laser cavity was folded using the concave mirrors ($r = 1$ m) M1 and M3 and the flat mirror M2. The output coupler (OC) defined the laser cavity length of 226 cm ± 1 cm. Two output couplers of 53% and 15% at $\lambda = 1064$ nm were used during mode-locked operation tests. The laser output beam was supplied to the analysis section of the setup by the flat high-reflectivity mirror M4. A diffractive beam splitter (DBS) was used to split the laser beam to a photodiode (PD), a power meter, and an optical spectrum analyzer. The zero-order diffraction beam was directed to the power meter. One of the first-order diffraction beams was directed to a photodiode (PD). The PD supplied the electrical signal to the analog oscilloscope and the triggering signal to the fast oscilloscope. The other first-order diffraction beam was coupled into a fiber by the use of a focusing lens L5, and supplied the signal to the optical spectrum analyzer. A wedge was used to supply a single surface reflection beam to the optical input of the fast oscilloscope, using a coupling lens L4 to focus onto the fiber. The optical spectrum analyzer was an Advantest model Q8384 with the measurement range 600–1700 nm, and with a wavelength measurement accuracy of the order of 0.1 nm[1]. The analog oscilloscope used was a Tektronix 7104, and was supplied with the electrical signal from a New Focus model 1611 InGaAs 1 GHz photodiode. The same photodiode was used to supply the triggering signal to the fast oscilloscope, an Agilent model 86100A. The Agilent oscilloscope was equipped with the optical module 86109A that allows optical input and has a 30-GHz bandwidth, with a measurement range of 1000–1600 nm.

5 Nd:YVO_4 laser mode locking with the QD-SAM

Firstly, the laser setup was optimized for cw operation at $\lambda = 1064.6$ nm. We have obtained 11-W output average power when a 53% OC was used, and when 42 W of pump power was supplied. This corresponds to a 26.2% laser system external efficiency. When the laser mirror was replaced with our QD-SAM, the laser switched from cw operation to self-starting stable cw mode-locked operation. The beam waist occurring at the position of the QD-SAM was slightly elliptical

[1] The calibration of the Advantest optical spectrum analyzer was checked with a helium–neon laser that operates at 1152.59 nm and the wavelength measurement accuracy is estimated to be 0.1 nm.

with horizontal diameter $d_h = 671\,\mu m$ FWHM and vertical diameter $d_v = 749$ um FWHM. The spot size measurements were based on the knife-edge technique, where a partially reflecting mirror was placed in the position of the QD-SAM and the spot size was measured on the back of the mirror.

During mode-locked laser operation the analog oscilloscope was used to monitor the stable cw mode-locked pulse train, while the fast oscilloscope monitored the pulse width and shape. Figure 4 shows the analog oscilloscope traces for the cw mode-locked laser operation, when a 53% OC was used. In the inset of Fig. 4 is the enlarged image of a group of two pulses. It can be seen that the pulse period is in agreement with the cavity round trip time, and hence the mode-locked operation corresponds to only a single pulse in the resonator cavity (laser operates in single-pulse regime). In Fig. 4, oscillations in the pulse tail are electrical in origin due to the detection system.

The pulse width and pulse bandwidth were simultaneously analyzed and recorded by the use of the fast oscilloscope and optical spectrum analyzer. The accurate determination of the pulse repetition rate was made with the fast oscilloscope. For the case when a 53% OC was used, mode-locked pulses measured on the oscilloscope were as short as $\Delta t = 36$ ps (Fig. 5) and had a spectral width of $\Delta\lambda = 0.06$ nm (Fig. 6) at the center wavelength of 1064.6 nm. The resultant time–bandwidth product $\Delta f\,\Delta t$ was 0.58, and represents 1.3 times the transform limit for Gaussian pulses [17]. The average output power was 7.1 W at a repetition rate of 65 MHz, which gives a pulse peak power of 3 kW. The optical pump power supplied was 40.9 W, and the optical to optical efficiency was 17.2%. From these measurements, the fluence incident on the QD-SAM was estimated to be $42\,\mu J/cm^2$. The reduced external efficiency from 26.2% in cw operation to 17.2% in mode-locked operation can be caused by the nonsaturable losses introduced by the QD-SAM, or by insufficient saturation of the QD structures.

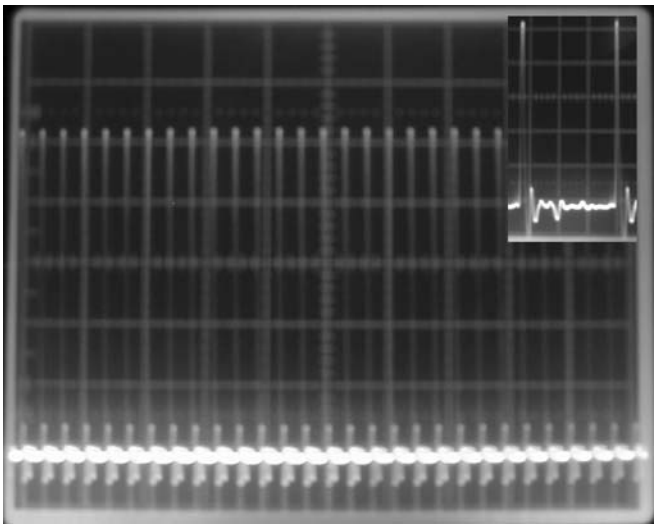

FIGURE 4 Analog oscilloscope trace of the cw mode-locked pulse sequences (50 ns/div time scale); the *inset* shows the magnification of two pulses (5 ns/div time scale)

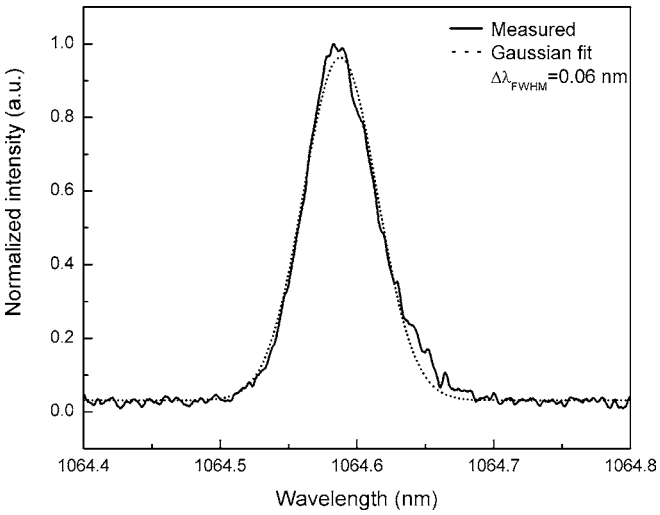

FIGURE 6 Optical spectrum of the pulses from the Nd:YVO_4 laser with the 53% output coupler, when passively mode locked by using the QD-SAM

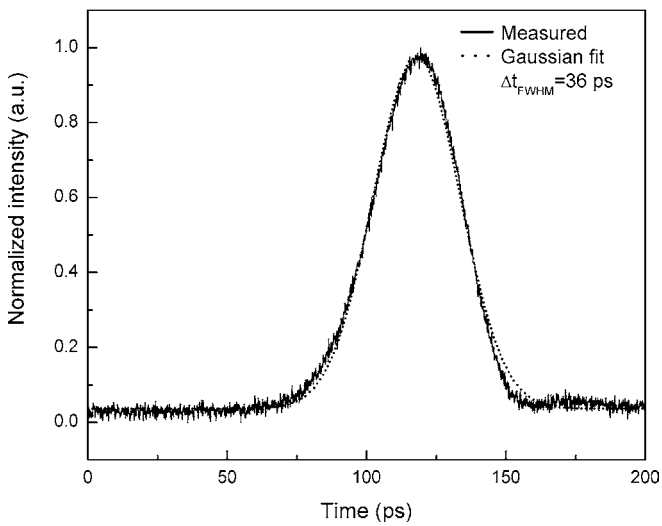

FIGURE 5 Measured pulse shape when the Nd:YVO_4 laser was operated with the 53% output coupler and the QD saturable absorber

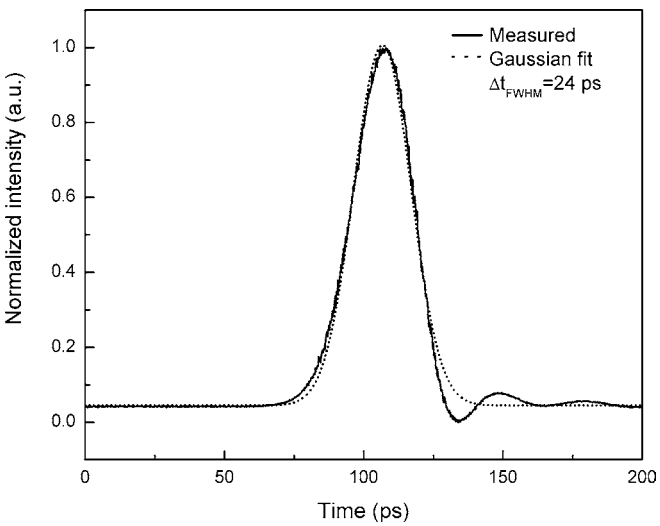

FIGURE 7 Measured pulse shape when the Nd:YVO_4 laser was operated with the 15% output coupler and the QD saturable absorber

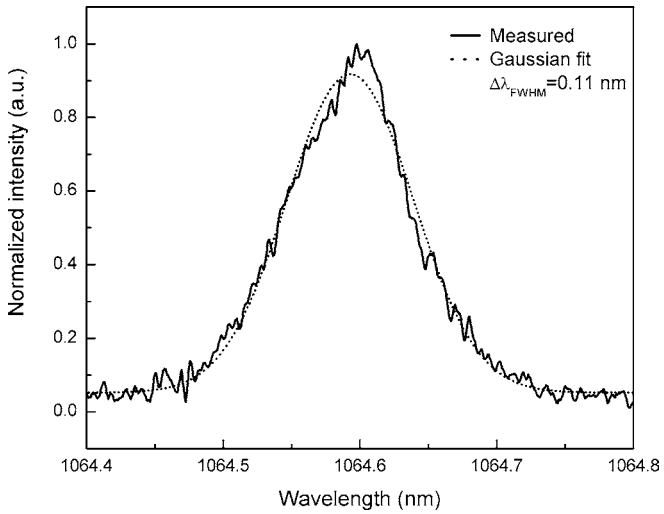

FIGURE 8 Optical spectrum of the pulses from the Nd:YVO_4 laser with the 15% output coupler, when passively mode locked by using the QD-SAM

For the case when a 15% OC was used, pulses as short as $\Delta t = 24$ ps, as measured on the oscilloscope (Fig. 7), with a spectral width of $\Delta\lambda = 0.11$ nm (Fig. 8) at the center wavelength of 1064.6 nm were obtained. In this case the time–bandwidth product was 0.70, or 1.6 times a transform-limited Gaussian pulse. We expect that this measurement is somewhat limited by the oscilloscope bandwidth (30 GHz) and the real pulse width would be of the order of 20 ps if a simple deconvolution of the oscilloscope bandwidth is applied. As the pulse bandwidth is 0.11 nm, and assuming transform-limited Gaussian pulses, the minimum pulse width that could be obtained would be 15 ps. The average output power was 1.94 W at a repetition rate of 65 MHz, which translates into a peak pulse power of 1.23 kW. The optical pump power supplied was 41.7 W, and the optical to optical efficiency was 4.6%. From these measurements, the fluence incident on the QD-SAM was estimated to be 55 $\mu J/cm^2$.

The mode-locked pulse width Δt is roughly proportional to $1/N$, where N is the number of laser cavity longitudinal modes that participate in the mode-locked operation (the modes that are phase locked). As expected, when the transmission of the output coupler was reduced, the cavity losses were reduced leading to a reduction of the lasing threshold, and in this way more longitudinal modes from the gain spectrum participated in the lasing operation. This leads to the generation of shorter pulses (24 ps) when the 15% OC was used, compared with the 36-ps pulse width when the 53% OC was used. Analyzing the pulse bandwidth for the 15% OC it can be seen that $\Delta\lambda = 0.11$ nm, which is almost double the pulse bandwidth of $\Delta\lambda = 0.06$ nm obtained for the 53% OC. This broadening in the pulse bandwidth with reduction in the output coupling is consistent with the results observed.

The laser output transverse mode was analyzed by using a CCD camera indicating a slightly elliptical spot with a beam diameter ratio of 1.2 and near-Gaussian profiles in the two transverse directions. The near-Gaussian output mode, combined with the short pulses and the multi-kW peak power, make this type of system a good candidate for material processing applications.

The use of the MBE technique to fabricate the QD-SAM without substrate rotation during growth gave the possibility of obtaining a large range of parameters for the QD-SAM across the wafer. In this work we have presented the mode-locked operation of one particular area of the wafer, where the QD-SAM had the optimum desired reflectivity and absorption for mode-locked operation for a Nd:YVO_4 laser at 1064.6 nm. Further analysis and tests are planned on lasers with broader gain bandwidths and at different wavelengths in the potential operating range of 970–1090 nm [9] of the present QD sample.

6 Conclusions

In conclusion, we have demonstrated self-starting, stable cw mode-locked operation of a grazing incidence slab Nd:YVO_4 laser at $\lambda = 1064.6$ nm using an InAs/GaAs QD-SAM. Mode-locked pulses as short as 24 ps with a repetition rate of 65 MHz were obtained with multi-watt laser output average power. Our present work indicates that the InAs/GaAs QD-based structures can be used as saturable absorbers for passive mode locking Nd-doped lasers at 1064 nm.

ACKNOWLEDGEMENTS We would like to gratefully acknowledge financial support from MPB Technologies Inc., the Natural Sciences and Engineering Research Council of Canada (NSERC), and the Canadian Institute for Photonic Innovations (CIPI). Z.Y. Zhang would like to acknowledge financial support from the Alberta Ingenuity Fund.

REFERENCES

1 O. Okhotnikov, A. Grudinin, M. Pessa, New J. Phys. **6**, 177 (2004)
2 M.J. Lederer, V. Kolev, B. Luther-Davies, H.H. Tan, C. Jagadish, J. Phys. D Appl. Phys. **34**, 2455 (2001)
3 L. Zhang, T.F. Boggess, D.G. Deppe, D.L. Huffaker, O.B. Shchekin, C. Cao, Appl. Phys. Lett. **76**, 1222 (2000)
4 A. McWilliam, A.A. Lagatsky, C.T.A. Brown, W. Sibbett, A.E. Zhukov, V.M. Ustinov, A.P. Vasil'ev, E.U. Rafailov, Opt. Lett. **31**, 1444 (2006)
5 R. Herda, O.O. Okhotnikov, E.U. Rafailov, W. Sibbett, P. Crittenden, A. Starodumov, IEEE Photon. Technol. Lett. **18**, 157 (2006)
6 K.W. Su, H.C. Lai, A. Li, Y.F. Chen, K.F. Huang, Opt. Lett. **30**, 1482 (2005)
7 A.A. Lagatsky, E.U. Rafailov, W. Sibbett, D.A. Livshits, A.E. Zhukov, V.M. Ustinov, IEEE Photon. Technol. Lett. **17**, 294 (2005)
8 E.U. Rafailov, S.J. White, A.A. Lagatsky, A. Miller, W. Sibbett, D.A. Livshits, A.E. Zhukov, V.M. Ustinov, IEEE Photon. Technol. Lett. **16**, 2439 (2004)
9 Z.Y. Zhang, C. Scurtescu, M.T. Taschuck, Y.Y. Ysui, R. Fedosejevs, M. Blumin, I. Savelyev, S. Yang, H.E. Ruda, Proc. SPIE **6343**, 63 432 (2006)
10 M. Blumin, H.E. Ruda, I.G. Savelyev, A. Shik, H. Wang, J. Appl. Phys. **99**, 093 518 (2006)
11 A. Polimeni, A. Patane, M. Henini, L. Eaves, P.C. Main, S. Sanquinetti, M. Guzzi, J. Cryst. Growth **201–202**, 276 (1999)
12 Z.Y. Zhang, Z.G. Wang, B. Xu, P. Jin, Z.Z. Sun, F.Q. Liu, IEEE Photon. Technol. Lett. **16**, 27 (2004)
13 J. Bass, J.S. Dugdale, C.L. Foiles, A. Myers, *Landolt-Bornstein*, vol. 15b (Springer, Berlin, Heidelberg, 1985)
14 J.E. Bernard, A.J. Alcock, Opt. Lett. **18**, 968 (1993)
15 A.J. Alcock, J.E. Bernard, IEEE J. Sel. Top. Quantum Electron. **3**, 3 (1997)
16 M.J. Damzen, M. Trew, E. Rosas, G.J. Crofts, Opt. Commun. **196**, 237 (2001)
17 K.J. Kuhn, *Laser Engineering*, 1st edn. (Prentice Hall, Englewood. Cliffs, NJ, 1997), chapt. 6